Processing, Structure, and Properties of Multiwalled Carbon Nanotube/Poly(hydroxybutyrate-*co*-valerate) Biopolymer Nanocomposites

Yanxuan Ma,[1] Yudong Zheng,[1] Guangye Wei,[1] Wenhui Song,[2] Te Hu,[1] Huai Yang,[1] Rundong Xue[1]

[1]*Research Center of Biomedical Materials, School of Materials Science and Engineering, University of Science and Technology Beijing, Beijing 100083, People's Republic of China*
[2]*Wolfson Center for Materials Processing, School of Engineering and Design, Brunel University, West London UB8 3PH, United Kingdom*

Received 24 February 2011; accepted 13 September 2011
DOI 10.1002/app.35650
Published online 6 February 2012 in Wiley Online Library (wileyonlinelibrary.com).

ABSTRACT: Biopolymer nanocomposites of carbon nanotubes (CNTs) which reinforced poly(hydroxybutyrate-*co*-valerate) (PHBV) were developed. Multiwalled carbon nanotubes were modified by an acid oxidation treatment (A-MWCNTs) to improve their dispersal in the polymer. The thermal properties, crystallization behavior, microstructure, and cross-sectional morphology of the composites were investigated. Their mechanical properties and surface contact angles were tested. The cytotoxicity of the composites to murine fibroblast L929 cells was also evaluated. The results show that A-MWCNTs are homogeneously dispersed in PHBV which demonstrate strong heterogeneous nucleation on the dynamics and kinetics of crystallization of PHBV. With the addition of A-MWCNTs, the crystallization temperature, heat of crystallization, and thermal stability of the composites increase. Consequently, the mechanical properties of the composites have been substantially improved. The composites become hydrophilic and have no obvious toxicity to the murine fibroblast L929 cells when the content of A-MWCNTs is below 1.5 wt %. © 2012 Wiley Periodicals, Inc. J Appl Polym Sci 125: E620–E629, 2012

Key words: composites; multiwalled carbon nanotubes; active groups; crystallization; property

INTRODUCTION

As a biopolymer, poly(hydroxybutyrate-*co*-valerate) (PHBV) has many attractive properties, such as degradability, biocompatibility, and its natural origin of bacterial fermentation.[1–3] In combination with its piezoelectric and optically active properties, it can potentially be used in the applications of prosthesis of soft and hard tissues, artificial organs, and artificial vessels. However, these applications are restricted by such problems as poor mechanical properties and lack of hydrophilicity. The use of fibers or nanoparticles as reinforcements or additives is an important and effective method to improve the mechanical properties and many other physical properties of polymers. It is well known that the fibers or nanomaterials with high strength and modulus predominantly contribute to the overall enhancement of mechanical performance of composites. Some native cellulose fibers and inorganic materials have been used to modify PHBV to increase its mechanical properties,[4–9] but the dispersal of the reinforcement and the interface between the reinforcement and the PHBV matrix are still open issues which limit the improvement in its mechanical properties.

Carbon nanotubes (CNTs) are promising as biomedical materials *in vivo*.[10–13] There are many reports concerning CNTs used as reinforcement,[14–18] and their improvement of the polymer's mechanical properties to various degrees. Some efforts have been made on development of the composites of CNT and PHBV,[18–20] with main focuses on the thermal behavior, morphology, and physical properties of the composites. Lai et al.[18] reported the nucleant effect of MWNTs on crystallization of PHBV and enhanced thermal stability from one type of formulation of composite containing 2 wt % of acid-treated MWCNTs made by carbon-arc process. More recent work[19] demonstrated thermal behavior, thermal/electrical conductivity, water uptake, and permeability of PHBV composites containing a range of MWCNTs (CVD growth, Baytues) from 1, 3, 5, to 10 wt %. Apart from the different synthesis, purification and surface treatment of carbon nanotubes in these two papers, it should be mentioned that PHBV

Correspondence to: Y. Zheng (zhengyudong@mater.ustb.edu.cn) or W. Song (wenhui.song@brunel.ac.uk).

used in their study was made by different manufacturers with different mol % of valerate and molecular weight. More intriguingly, some abrupt changes of several physical properties of MWCNT-PHBV composites with MWCNT content in the low range (at 1 or 3 wt %) were observed,[19] indicating that more data on the structure–properties in the composites with low nanotube contents are still needed for further understanding the role of carbon nanotubes in PHBV matrix and optimization of the composite design and process. Clearly, a systematic study on the properties, especially mechanical properties and biocompatibility, and further establishment of the relationship between the structure and properties of such composites are still highly desirable. Because of the strong hydrophobic interaction between them and their large specific surface area, the CNTs tend to entangle, bundle and agglomerate, thus they are difficult to disperse evenly in polymer matrices. Great effort has been made to find suitable solvents, surfactants, various covalent, or noncovalent modifications of the CNT surfaces in order to separate the CNT agglomerates or bundles within different types of polymer matrices. Nevertheless, except superacid and chlorosulfonic acid, there is no common organic solution to disperse CNTs effectively.[21] Among various surface modification approaches, the oxidation of CNT surfaces by a mixture of strong acids is often applied.[22,23] In this study, acid-treated MWCNT (A-MWCNT) reinforced PHBV (A-MWCNT/PHBV) composites were made from dispersion by ultrasonication and conventional solvent-casting.[24] We investigated a series PHBV composites containing a range of low concentration of nanotubes aiming to develop biocompatible PHBV nanocomposites and understand the reinforcement contributed by the nanotubes. The dispersal of MWCNTs before and after acidification, the microstructure and cross-sectional morphology of the composites were observed. The thermal properties and crystallization behaviors of the composites were measured. The mechanical properties, including the elastic modulus, tensile strength and fracture elongation, as well as surface contact angle were tested. The cytotoxicity of the composites to the murine fibroblast L929 cells was also evaluated.

EXPERIMENTS

Materials

MWCNTs, Short-MWCNT-4060, length 1–2 μm, amorphous<3%, were bought from Shenzhen Nanotech Port PHBV, HB-*co*-21%HV, granularity Dp300, was purchased from Biopol Chloroform, analytically pure, density 1.471–1.481, was provided by Beihua Fine Chemicals Limited in Beijing. Concentrated sulphuric acid, concentrated nitric acid and deionized water were also used.

Acidification and measurements of MWCNTs

A mixture of concentrated H_2SO_4:HNO_3 acid was made with a volume ratio of 3 : 1. Certain amounts of MWCNTs were suspended into the acid mixture, which was refluxed in a water bath for 3 h at a temperature of 80°C. The resultant suspension was cooled down to the room temperature for another hour, and then centrifuged after adding the deionized water into it in order to remove the remaining acid from the suspension until pH of the suspension liquid reached 7.20. The A-MWCNTs were dried at 60°C in an oven for 24 h to evaporate all the remaining water. And then, the A-MWCNTs were manually ground into powders in a grinding bowl for 15 min.

The untreated MWCNTs and A-MWCNTs, with a weight concentration of 1.0 wt %, were weighed and suspended in deionized water separately. The suspensions were sonicated in an ultrasonication water bath for 15 min under a power of 150 W. The stability of both untreated and acid-treated CNT suspensions in the test tubes was compared after 60 h.

The morphology of the MWCNTs before and after acidification was observed using a field emission scanning electron microscope (FESEM, Zeiss SUPRA™55). The diameter and length of the untreated and acid-treated nanotubes were measured by IMAGE software from FESEM images, where separated nanotubes were prepared by casting a dilute dispersion on a polished SEM stub and drying at room temperature. The dimensions quoted for each sample were the average of measurements on over 100 individual nanotubes.[25]

Preparation of the composites

The PHBV was dissolved into the chloroform with a concentration of 25 g/L and refluxed for 1 h in a water bath at a temperature of 90°C. A-MWCNTs were added into the deferent solutions with A-MWCNT/PHBV contents of 0.0, 0.5, 1.0, and 1.5 wt %. After ultrasonication for 5 min with a power of 200 W, the suspensions were cast into culture dishes and tensile test bar moulds separately. Most of the solvent was evaporated at a temperature of 70°C after 24 h. The resulting composites, thickness 2 mm, were kept dry at room temperature.

Characterization

The composites were cut into specimens of 10 × 10 mm^2 square sheets. The sheet was mounted into resin and then cut through. The cross section at cut

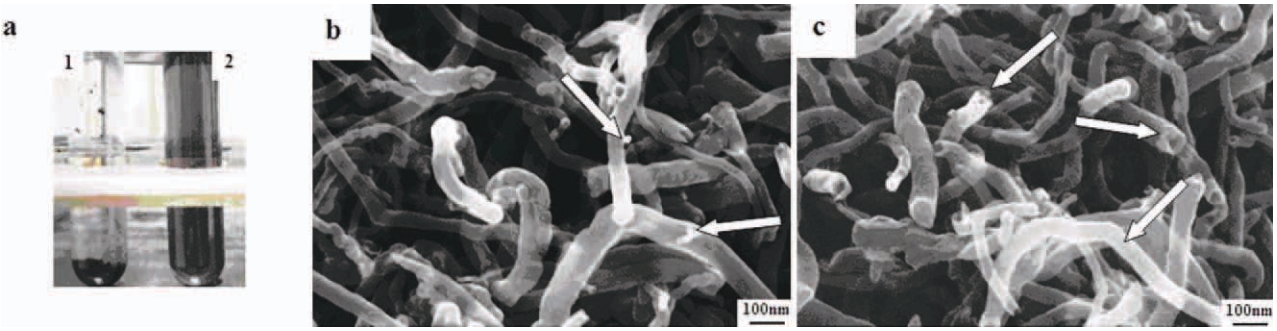

Figure 1 Acidification of MWCNTs: (a) Precipitation situation of suspensions after 60 h: (1) Untreated MWCNTs and (2) A-MWCNTs; SEM images of (b) Untreated MWCNTs, and (c) A-MWCNTs. [Color figure can be viewed in the online issue, which is available at wileyonlinelibrary.com.]

surface of the specimen was carefully ground and polished. After coated with a thin layer of gold, the cross-sectional morphology was examined by FESEM. Wide angle X-ray scattering was done on a X Ray-diffractometer (XRD, D/MAX–RB12KW,Cu target), operated at a continuous $2\theta/\theta$ coupled scan with a step width of 0.02° and a working voltage 40 kV. The thermal properties were tested by a differential scanning calorimeter (DSC, Perkin-Elmer DSC-6, US). The weight of each sample was 3.5 mg. The samples of the pure PHBV and A-MWCNT/PHBV composites were first heated from room temperature to 200°C at a heating rate of 30°C/min, and then held at 200°C for 5 min in order to eliminate their thermal history. The rate of subsequent cooling scan and reheating scan was 10°C/min.[22]

The samples were prepared by solution-cast for tensile mode mechanical tests with dimensions of length 44 mm, width 6 mm and thickness 2 mm. With a stretching rate of 2.00 mm/min, the mechanical properties of the composites, such as the elastic modulus, the tensile strength and the fracture elongation, were tested using a WDS series microcomputer control electronic universal testing machine (Rising Sun Testing Instrument, Changchun China). All the property data were obtained by averaging the test results of five samples. The stress-load curves, fracture elongation, tensile strength, stress–strain curves, and elastic moduli were analyzed and calculated. Five samples were used at test point; the error bars in Figure 5 represented standard deviation.

The films of pure PHBV and A-MWCNT/PHBV composites were cut into specimens with dimensions of 10×10 mm^2, clung to glass slides and put on the specimen stage of Contact Angle System 15 Plus (DataPhsycs GmbH, Germany). The surface contact angle was tested using the drop method at a speed of 1 μL/s. Five samples were used at test point; the error bars in Figure 6 represented standard deviation.

The cytotoxicity of the composites was evaluated by the method of direct contact following ISO 10993-5: 1999. Murine fibroblast L929 cells were put into the cultural fluid for 24 h. The specimens (600 mm^2 in area) of the A-MWCNT/PHBV composites (pure PHBV, A-MWCNT/PHBV of 0.5, 1.0, and 1.5 wt %) were initially sterilized. Then the samples were put on the cell layers, with the blank group containing only the fresh cultural fluid and the positive group with 5 wt % dimethylsulfoxide in the fresh cultural fluid, for two, four, and seven days. The growth conditions of the cells were observed at different time. The numbers of the cells in the experimental group and blank group were counted and the relative growth rates (RGR) were calculated with the following equation:

$$\text{Relative growth rate} = \frac{\text{Average number of cells in the experimental group}}{\text{Average number of cells in the blank group}} \times 100\%$$

RESULTS AND DISCUSSION

The acidification effects

Figure 1(a1,a2) compare the precipitation situation of aqueous suspensions of untreated and acid-treated MWCNTs after leaving for the same period of time (60 h). As expected, untreated MWCNT agglomerates were clearly seen at the bottom of the test tube in Figure 1(a1). In fact, due to the hydrophobic nature of graphene wall surfaces and impurities in the original MWCNTs, these MWCNTs clustered easily and the suspension was not stable once the ultrasonication was stopped. The precipitation appeared within 20 min. However, the A-MWCNT suspension was much more stable [shown in Fig. 1(a2)], which could last for at least four months in this study without the appearance of precipitation, or even longer depending on the degree of the acid oxidation. The stable aqueous suspension is attributed to the

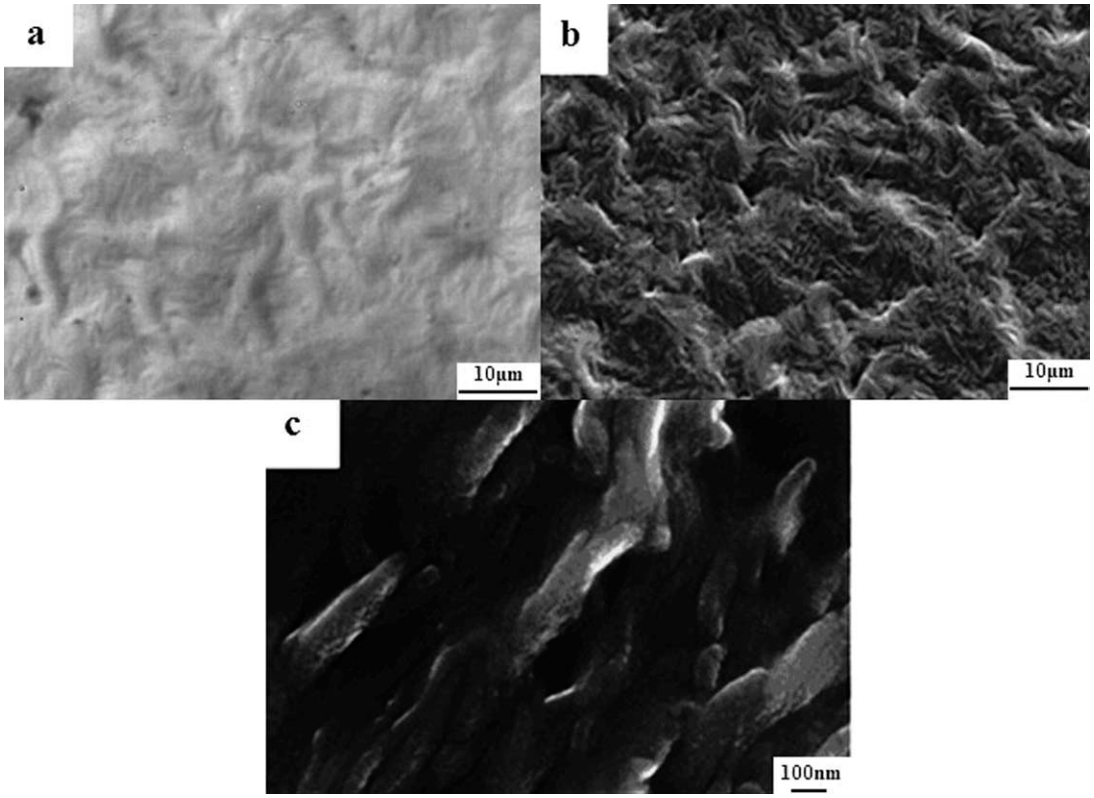

Figure 2 SEM images of the cross section morphology of (a) pure PHBV; and (b) and (c) A-MWCNT/PHBV (1.0 wt %) composite at different magnifications.

functionalized CNT surfaces, grafted by the hydrophilic hydroxy and carboxyl groups.[26,27]

The morphology of the untreated and acid-treated MWCNTs is presented in Figure 1(b,c). The untreated MWCNTs appeared to entangle together with some impurity particles clinging to their surfaces, as shown by the arrows in Figure 1(b). The average aspect ratio (length/diameter ratio) of the untreated MWCNTs was about 100, while their diameters were various, ranging from 20 to 120 nm. After acid oxidation, the A-MWCNTs became less entangled with the appearance of thinner, shorter, and straighter CNTs with many open tube ends, as shown by the arrows in Figure 1(c). As a result, the average aspect ratio of the A-MWCNTs became smaller by a factor of 10, and the distribution of their diameters got narrower, with an average diameter of about 80 nm. In addition, the impurity particles were removed during the acid oxidation process.

Cross-sectional morphology

Figure 2 reveals the morphology of pure PHBV and A-MWCNT/PHBV (1.0 wt %) composite sheets by

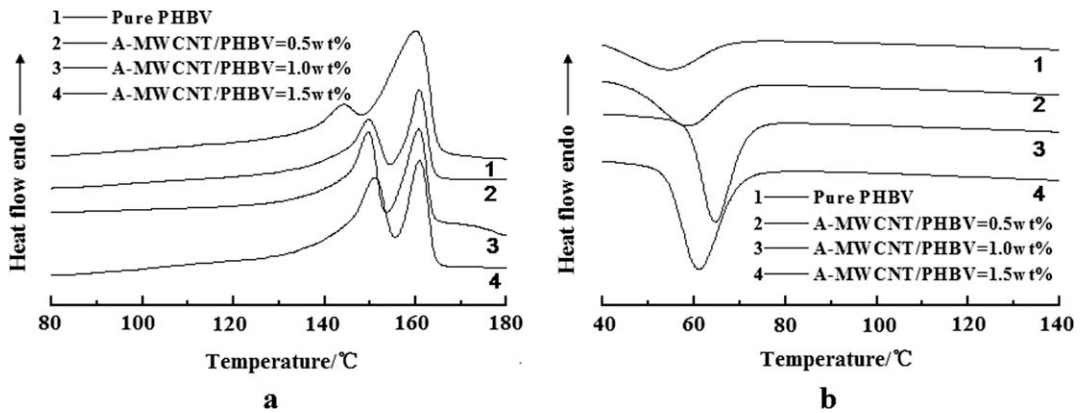

Figure 3 DSC heating curves (a) and cooling curves (b) of pure PHBV and A-MWCNT/PHBV composites with different A-MWCNT contents.

TABLE I
Thermal Parameters of Pure PHBV and A-MWCNT/PHBV Composites

A-MWCNTs/ PHBV (wt %)	T_{m1}/°C	T_{m2}/°C	T_c/°C	T_{on}/°C	T_f/°C	$\Delta T(1/2)$/°C	ΔH_c/J g^{-1}
0.0	144.3	159.9	54.7	69.1	37.8	15.6	13.51
0.5	149.7	160.7	58.8	71.8	42.4	14.7	15.24
1.0	149.8	160.8	64.7	76.3	55.6	7.4	21.67
1.5	150.9	161.1	61.1	74.8	50.6	12.1	26.89

T_{m1}, the first endothermic peak temperatures during heating; T_{m2}, the second endothermic peak temperatures during heating; T_c, the exothermic peak temperatures during cooling; T_{on}, the onset starting temperatures of the exothermic peak during cooling; T_f, the final temperatures of the exothermic peak during cooling; ΔT (1/2), temperature width of the exothermal peaks at half-peak height; ΔH_c, the crystallization heats measured during cooling.

field emission scanning electron microscopy. It shows that the typical spherulites consisting of lamellar fibril bundles parallel to the radial direction formed in pure PHBV during the casting in Figure 2(a). Compared with the morphology of cross section of pure PHBV in Figure 2(a), similar but denser spherulite-like morphology appeared in the A-MWCNT/PHBV (1.0 wt %) composite, as shown in Figure 2(b). The hydrogen bonds are believed to form between the PHBV matrix and A-MWCNTs grafted by the active groups. As expected, A-MWCNTs were well dispersed in the PHBV chloroform solution. After solvent evaporation, the composites consist of a nanofibrous structure with a globally random orientation. From the close-up image of Figure 2(c), the fibrils appear to grow locally into bundles along certain orientations and extend radially in the same way as lamellar fibrils of the spherulites in pure PHBV, as shown in Figure 2(a,b). The diameter of the fibrils or fibril bundles is around 100 nm, slightly thicker than the A-MWCNTs themselves. It is envisaged that the A-MWCNTs with only 1.0 wt % would act as crystal nucleuses which induce PHBV crystals to grow into more and smaller spherulites in the composites. The uniformity of the fibrils and distribution of the spherulites reflects that the A-MWCNTs are embedded and well distributed in the polymer matrix. The following study on the thermal behaviors and crystalline structure of the composites provide more insight into the role of carbon nanotubes in the crystallization of the composites.

Crystallization behaviors

The crystallization behaviors and crystalline structure were investigated using DSC and XRD. First, Figure 3 shows the DSC heating curves and cooling curves of the composites with different compositions at a scanning rate of 10°C/min. Curve 1 of Figure 3(a) is the heating curve of pure PHBV showing two melting peaks with T_{m1} at 144.3°C and T_{m2} at 159.9°C. With the presence of A-MWCNTs, the two melting peaks become sharper, and shift to higher temperatures. The up-shift trend of the first melting point (T_{m1}) more or less levels off with an increase in the A-MWCNT content, as shown in the heating Curves 2, 3, and 4 of Figure 3(a). The melting temperature data are summarized in Table I.

The cooling curves in Figure 3(b) demonstrate the nonisothermal crystallisation behaviours of the composites with different A-MWCNT contents in comparison with pure PHBV. The related thermal analysis parameters obtained from the cooling curves are listed in Table I. It is clear that the presence of A-MWCNTs changes the dynamics and kinetics of nonisothermal crystallisation of the composites. From Figure 3(b) and Table I, the presence of the A-MWCNTs increases the crystallisation temperature (T_c) of the composites as compared with pure PHBV. The increase is more obvious at a low content of the A-MWCNTs (0.5 and 1.0 wt %), but appears to slow down when the A-MWCNT content becomes higher (1.5 wt %). The width of the crystallisation peaks defined as the temperature difference at half-peak height, ΔT (1/2), indicates the crystallization rate in the nonisothermal crystallisation process. Similar to the trend of the melting temperature, the crystallization of the composites speeds up with an increase in the A-MWCNT content, but quickly peaks at 1.0 wt % A-MWCNTs showing a sharp exothermal peak with its $\Delta T(1/2)$ less half of that for pure PHBV in Table I. Compared with PHBV, the crystallization heat (ΔH_c) of the composites calculated from Figure 3(b) increases continuously with an increase in the A-MWCNT content up to 1.5 wt %, implying that growth of crystallinity in the composites.

Figure 4 shows the XRD patterns of pure PHBV and the A-MWCNT/PHBV composites. The diffraction patterns for both the PHBV and the A-MWCNT/PHBV composites are similar, corresponding to the orthogonal space Group P_{212121} crystalline structure, which is the typical crystal conformation of PHBV.[28,29] The full with at half maximum (FWHM) of diffraction peaks of their crystal planes

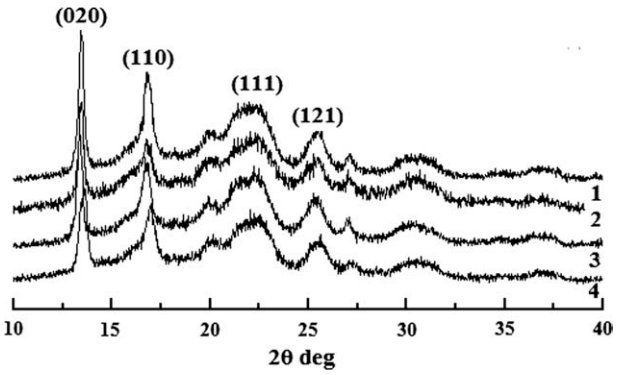

Figure 4 XRD patterns of the A-MWCNT/PHBV composites with different A-MWCNT contents: (1) 0.0 wt %, (2) 0.5 wt %, (3) 1.0 wt %, and (4) 1.5 wt %.

were measured and listed in the Table II. With the addition of A-MWCNTs, a small increase of the FWHM of diffraction peaks of crystal planes of PHBV, (020), (110), (111), and (121), in the composites was observed. This means a decrease of the size of crystallites as the peak width is inversely proportional to crystallite size.

The combination of results of thermal analysis and XRD indicates that the presence of the A-MWCNTs in the composites does not change the crystal structure of the PHBV matrix, but affects the dynamics and kinetics of PHBV crystallization. The double melting peaks in the melting curves in Figure 3(a) have been proved to be the result of reorganization of the crystal structure of the poly-hydrobutyrate (PHB) and poly-hydroxyvalerate (PHV) units of the copolymer PHBV during the heating, whereby the two comonomer units cocrystallize in the same crystal lattice, a phenomenon known as isodimorphism.[30,31] Different from the pure PHBV with the predominant and broad endothermic melting peak at high temperature (T_{m2}), the two peaks of the composites become sharper and higher. The sharpening and up-shift of the first endothermic melting peak at low temperature (T_{m1}) are more distinct with an increase in the A-MWCNT content. This implies that the nucleating effect of the A-MWCNTs may assist the polymer chain packing and the formation of a uniform PHBV crystal structure, and therefore enhance the thermal stability of the composites.

Meanwhile the A-MWCNTs have a profound influence on crystallization characteristics. From Figure 3 and Table I, the increase of the crystallizing temperature and exothermic heat of crystallization of the composites imply different roles of the A-MWCNTs during the crystallization of PHBV. As long as the composite melt reaches the crystallization temperature, the A-MWCNTs are known to act as a large amount of heterogeneous nucleation sites, inducing PHBV crystallization. The sharp crystallization peak and substantial increase of the heat of crystallization of the composites with an increase of the content of A-MWCNTs, such as 100% increase (ΔH_c) in the case of the composite containing 1.5 wt % of A-MWCNTs, further proves that the A-MWCNTs promote the crystallization and uniformity of PHBV. Having described above, there is no obvious change in the crystal lattice structure of PHBV in the composites as compared to that of pure PHBV. This indicates that the nucleation effect of the A-MWCNTs has little influence on the direction of PHBV crystallite growth. However, the increase of the FWHM of diffraction peak of crystal planes of PHBV in the Figure 4 and Table II, as an diffraction effect of the decrease of the size of crystallites, further supports the above discussion on nucleation effect of A-MWCNT and the effect of carbon nanotube content on the melting and crystallization of the composites at nonisothermal conditions of DSC tests. The functionalization of the A-MWCNT surfaces and interfacial interaction between the A-MWCNTs and PHBV chains are speculated to influence the growth condition of the crystallites.

Mechanical properties

Figure 5 shows the stress–strain curves of the A-MWCNT/PHBV composites (a) and the effects of the A-MWCNT content on the elastic modulus, tensile strength and elongation to fracture of the composites (b). With an increase of the A-MWCNT content, the elastic modulus and tensile strength increased first and then peaked when the A-MWCNT content was around 1.0 wt %. In the case of the composites with 1.0 wt % A-MWCNTs, the elastic modulus rose to 297 MPa and the tensile strength to 6.98 MPa, with both around twice as high as those of pure PHBV. The elastic modulus of pure PHBV was 145 MPa, while the tensile strength was 3.61 MPa. There was a dramatic increase of the fracture elongation (0.083) of the composite, with the lowest A-MWCNT content (0.5 wt %), about a 232% increase as compared with pure PHBV (0.025). After reaching the yield strength, multistep yield behavior occurred during long elongation of the composite containing a low concentration (0.5 wt %) of the nanotubes, which may be attributed to the polymer

TABLE II
Full Widths at Half Maximum (FWHM) of Diffraction Peaks of Pure PHBV and A-MWCNT/PHBV Composites

A-MWCNTs/ PHBV (wt %)	FWHM (deg)			
	(020)	(110)	(111)	(121)
0.0	0.914	0.961	1.042	0.954
0.5	0.915	1.076	1.054	0.955
1.0	0.915	1.064	1.050	0.966
1.5	0.985	1.438	1.367	0.994

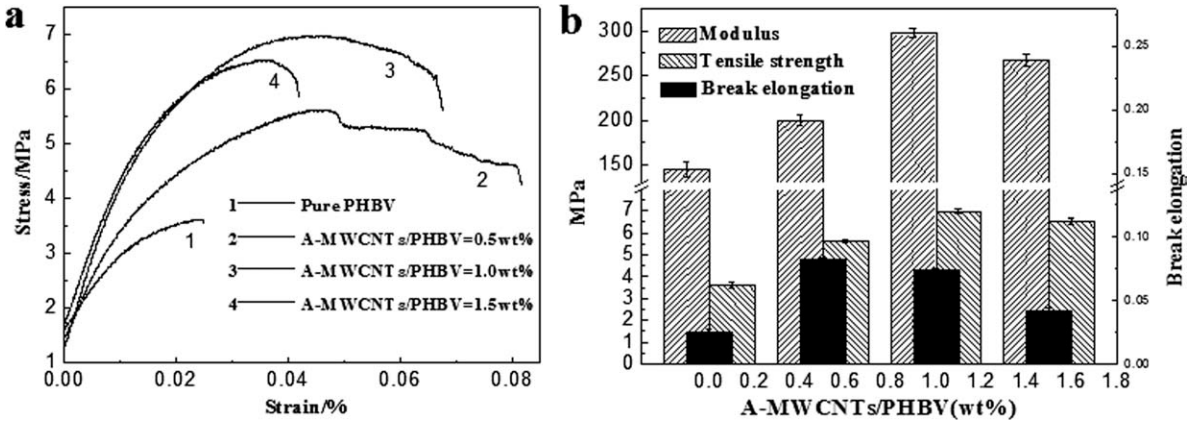

Figure 5 Typical stress–strain curves (a), elastic moduli, tensile strengths and elongations to fracture (b) of the A-MWCNT/PHBV composites with different A-MWCNT contents of 0.0, 0.5, 1.0, and 1.5 wt %.

chain movement and orientation accompanying with nanotube pull-out from PHBV matrix at the different stages of stretching. Together with the increases of strength and elastic modulus, the toughness of the composites was also substantially enhanced. It implies that uniform distribution of A-MWCNTs and strong interface between A-MWCNT and PHBV may contribute to the reinforcement significantly in the case of the low A-MWCNT content. However, the fracture strain of the composites started to drop with further increase of the A-MWCNT content. This indicated that the composites became stiffer but more brittle.

The results of the tensile tests demonstrate that the presence of a small amount of A-MWCNTs (<2 wt %) has greatly improved the mechanical performance of PHBV based composites. In practice, the reinforcement, contributed by the exceptionally high strength and modulus of individual A-MWCNT, is still far below theoretical expectation. From the trend of the improvement as a function of the A-MWCNT content, the interface between A-MWCNTs and PHBV, and the A-MWCNTs on the surrounding polymer are proposed to play different important roles. They have been proved both experimentally and theoretically in other composite systems.[32] In this study, the chemical groups, grafted on the surface of the MWCNTs through the acid treatment, not only facilitate a uniform dispersion of the MWCNTs within PHBV matrix, but also build up a strong interface between A-MWCNTs and PHBV. The abundant interfacial area at the nanoscale is essential for effective stress distribution and stress transfer between the A-MWCNTs and PHBV. On the other hand, the surface of the A-MWCNTs also means that a large proportion of the surrounding polymer chains are involved in the interface, with physical properties different from the bulk matrix. In the case of using crystalline polymer as the matrix, more uniform and smaller crystal structure of PHBV would grow, resulting from the A-MWCNT nucleating effects and surface confinement. The higher melting temperature of the composites, the stronger influence of the A-MWCNTs on the polymer matrix. In turn, the properties of the composites, especially those matrix and interface-dominated or related properties, are enhanced.

Similar to many other composite systems, the maximum improvement of mechanical properties of the A-MWCNTs reinforced composites is reached once the A-MWCNT concentration is above a certain percolation threshold. The formation of the percolation network of the A-MWCNTs is dependent on the A-MWCNT dispersal and interaction with the polymer matrix, and it determines the physical and mechanical properties of the A-MWCNTs. However, with more A-MWCNTs added, the competition between the separation and aggregation of the A-MWCNTs is bound to change. When the A-MWCNT content is increased above the percolation threshold, and the degree of the connectivity among the A-MWCNTs becomes higher, the A-MWCNTs tend to form more agglomerates. As a consequence, the surface of the A-MWCNTs, per unit volume fraction, and interface between A-MWCNTs and PHBV actually decrease. The improvement of the mechanical properties starts to reduce regardless of the increase in the A-MWCNT content. This further proves that the surface and interface of the A-MWCNTs are also primary parameters in determining the properties of the composites. The reinforcement, contributed from their own mechanical properties, does not always increase proportionally with the CNT content. It is beyond the prediction based on the rule of mixtures in the classical theory of fiber reinforced composites.

Hydrophicility

Figure 6 shows the measurement and calculation of the surface contact angles between A-MWCNT/

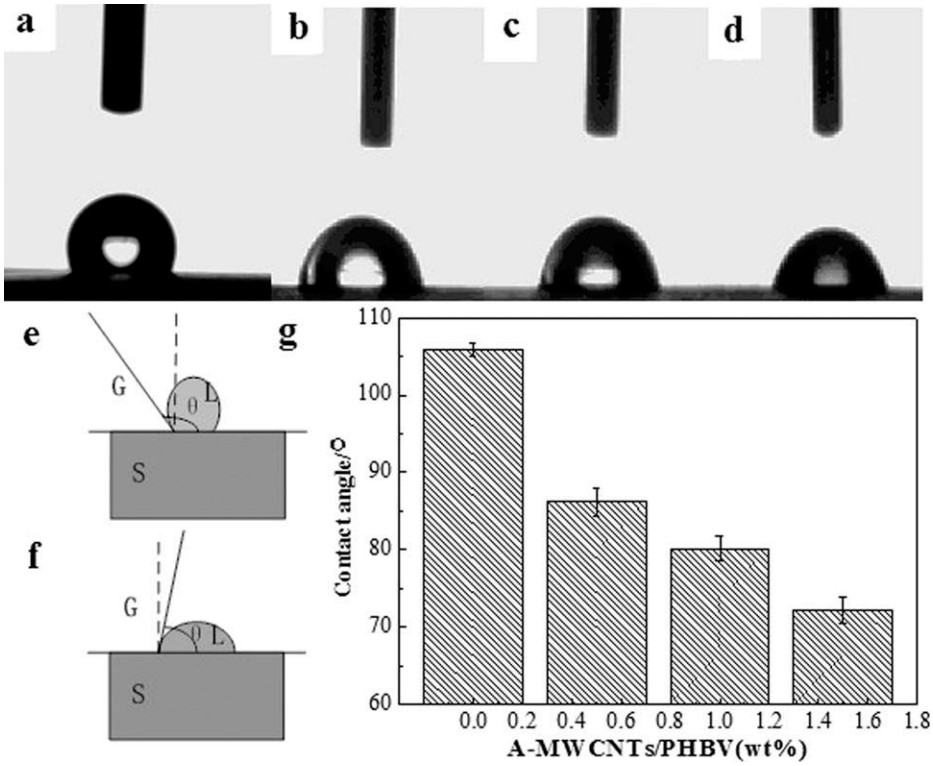

Figure 6 The measurement and calculation of the surface contact angle between A-MWCNT/PHBV composites with different contents of A-MWCNTs and deionized water: (a) pure PHBV, (b) the A-MWCNT content of 0.5 wt %, (c) the A-MWCNT content of 1.0 wt %, (d) the A-MWCNT content of 1.5 wt %, (e, f) schematics of the surface contact angle, (g) values of the surface contact angle versus the A-MWCNT content.

PHBV composites with different contents of A-MWCNTs and deionized water. Clearly, the surface contact angle of the composites decreased with an increase of the content of A-MWCNTs. With the A-MWCNT contents of 0.5, 1.0, and 1.5 wt %, the surface contact angle of the composites decreased to 86.20°, 80.11°, and 72.24°separately.

The surface state and hydrophilic performance of biomaterials have a major effect on the growth of the cells and tissues.[33] Following Young's equation,[34] with an increase of adherence tension and a decrease of liquid surface tension, the surface contact angle decreases. $\theta > 90°$ means that the surface is hydrophobic, while $\theta < 90°$ is the opposite, as shown in Figure 6(e,f). Possible factors, such as hydrophilicity of A-MWCNTs and PHBV, and surface roughness of the composites may contribute to the surface contact angle of the composites. As proved in our recent work,[35] the active groups grafted on the surface of A-MWCNTs during acidification have greatly improved the hydrophilicity of A-MWCNTs compared with untreated ones. From another aspect, those functional groups enhance the compatibility between A-MWCNTs and PHBV. As a result, the dispersed A-MWCNTs are most likely being wrapped or surrounded by PHBV macromolecular chains, which may cover the hydrophilicity of A-MWCNTs. Taking into account hydrophobic nature of PHBV, it is envisaged that surface roughness would be a predominate contributor to the decrease of contact angle of the composites with an increase of the A-MWCNT content. The addition of A-MWCNTs may have limited contribution to the increase the hydrophilicity of the composites

TABLE III
The RGR and Toxicity Grade of A-MWCNT/PHBV Composites and Positive Group

A-MWCNTs/ PHBV (wt %)	2 days		4 days		7 days	
	RGR	Toxicity grade	RGR	Toxicity grade	RGR	Toxicity grade
Positive groups	0.061952	4	0.053111	4	0.055194	4
0.5	0.995311	0	0.997122	0	0.991868	0
1.0	0.990602	0	0.993840	0	0.992576	0
1.5	0.991987	0	0.994476	0	0.981278	1

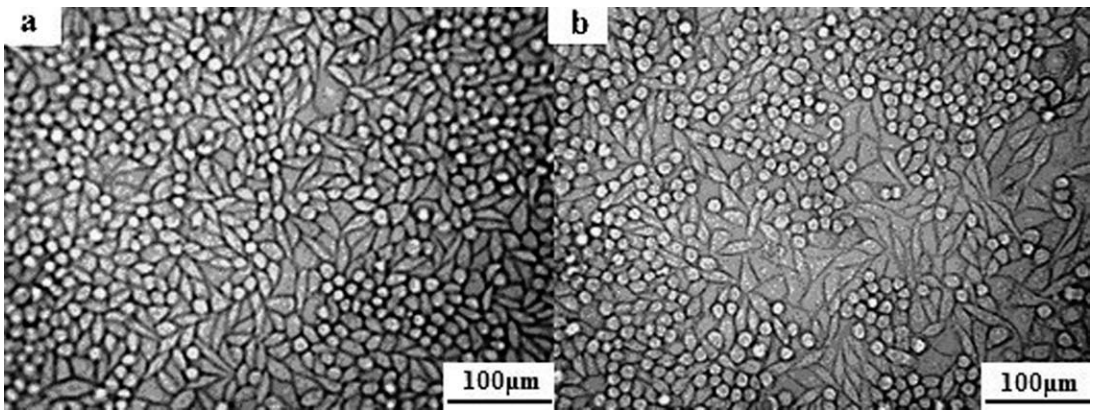

Figure 7 Morphology of murine fibroblast L929 cells culturing for four days on (a) Blank group, (b) A-MWCNT/PHBV (1.5 wt %) composite.

because of the possible shielding effect, but their nucleation effect induces different microstructure with smaller spherulites with more spherulite boundary (Fig. 2), and thus changes the surface roughness of the composites. For materials with a surface contact angle lesser than 90°, a large surface roughness provides more actual surface contact area, resulting in improved wettability of the material surface.[33] The above discussion can be further proved through more systematic measurements of the surface chemical composition, surface morphology and surface roughness of the composites in the future.

Cytotoxicity

The cytotoxicity test is an important method for biological evaluation. Due to the general applicability of *in vitro* cytotoxicity tests and their widespread use in evaluating a large range of medical devices and materials, ISO 10993-5:1999 defines a scheme for testing which requires to be made in a series of steps. Three categories of test are listed: extract-contact test, direct test, and indirect-contact test. The direct contact method is used to study cell morphology and RGR has the highest sensibility to the cytotoxicity of the material among the three methods. In this test, a direct contact method in ISO 10993-5: 1999 is used. United States Pharmacopoeia 27, which is not only one of the strictest technical requirements of drug quality standards and test methods, but also the legal basis of drug production, use, management, and inspection, is chose as standard of cytotoxicity. Table III summarizes the test results of the RGR and toxicity grade of A-MWCNT/PHBV composites and positive group to murine fibroblast L929 cells culturing on them. As shown in Table III, the RGR of all the A-MWCNT/PHBV composites to murine fibroblast L929 cells is high, and even in the case of the composite containing the highest content of A-MWCNTs 1.5 wt %, the RGR is still above 0.98 for seven days. The grades of toxicity of A-MWCNT/PHBV composites to murine fibroblast L929 cells range from Grade 0–1, which can classify such composites as eligibility for United States Pharmacopoeia 27(2004).

Figure 7 shows the morphology of murine fibroblast L929 cells culturing for four days on A-MWCNT/PHBV (1.5 wt %) composite and blank group. The cells were seen in shapes of irregular lozenges from Figure 6. When the A-MWCNT content was equal to or less than 1.0 wt %, the cytotoxicity of the composites was at level 0, which meant there was no cytotoxicity to the cells. When the A-MWCNT content was greater than 1.0 wt %, there was a slight suppression of the cell growth with the cytotoxicity at Level 1, but the RGR was still kept high at above 0.98. The reasons that the composite surface favors cells spreading and growth are supposed to be attributed to the increases of the surface hydrophilicity and surface roughness at the nanoscale of the composites containing A-MWCNTs. The reason for the minor decrease of cell growth over days in the test might have been the influence of residual chloroform in the composite from the solvent casting. Nevertheless, as the cytotoxicity remains between Levels 0 and 1, there is no obvious cytotoxicity of the A-MWCNT/PHBV composites to murine fibroblast L929 cells.

CONCLUSIONS

The hydroxy and carboxyl groups, grafted to the MWCNTs through the acid oxidation treatment, improve the dispersal and stability of MWCNTs in a PHBV matrix. There is a range of effects of the presence of A-MWCNTs on the structure, thermal and mechanical properties of PHBV based composites. The addition of the A-MWCNTs changes the crystallization mechanism, crystal growth dynamics, and kinetics of the PHBV matrix, such as 100% increase (ΔH_c) in the case of the composite containing 1.5 wt % of A-MWCNTs. The effect of heterogeneous

nucleation proves that the A-MWCNTs promote the crystallization of PHBV. A-MWCNTs at a low range of concentration (0.5–1.5 wt %) can improve the mechanical properties and hydrophilicity of the composites significantly. In the case of the composites with 1.0 wt % A-MWCNTs, the elastic modulus rose to 297 MPa and the tensile strength to 6.98 MPa, with both around twice as high as those of pure PHBV. There was a dramatic increase of the fracture elongation (0.083) of the composite, with the lowest A-MWCNT content (0.5 wt %), about a 232% increase as compared with pure PHBV (0.025). If the A-MWCNT content is further increased, the improvement reaches a threshold and then starts to decline. With the A-MWCNT contents of 0.5, 1.0, and 1.5 wt %, the surface contact angle of the composites decreased to 86.20°, 80.11°, and 72.24°separately. With low A-MWCNT content, $\leq$1.5 wt %, the A-MWCNT/PHBV composites have no obvious cytotoxicity to murine fibroblast L929 cells.

The study is financially supported by National Natural Science Foundation of China Projects (NO. 51073024), the Science and Technology Plan Project of Beijing, the Royal Society-NSFC International Joint Project Grant (NO. 51111130207), National Exemplary Center for Experimental Teaching of China and Brunel Research Development Fund.

References

1. Li, H. Y.; Chang, J. Polym Degrad Stab 2005, 87, 301.
2. Köse, G. T.; Korkusuz, F.; Korkusuz, P.; Purali, N.; Özkul, A.; Hasırcı, V. Biomaterials 2003, 24, 4999.
3. Zheng, Y. D.; Wang, Y. J.; Yang, H.; Chen, X. F.; Chen, Z. H. J Biomed Mater Res B 2007, 1, 236.
4. Godbole, S.; Gote, S.; Latkar, M.; Chakrabarti, T. Bioresour Technol 2003, 86, 33.
5. Sanjeev, S.; Mohanty, A. Compos Sci Technol 2007, 67, 1753.
6. Li, H. Y.; Chang, J. Biomaterials 2004, 24, 5473.
7. Wang, S. F.; Song, C. J.; Chen, G. X.; Guo, T. Y.; Liu, J.; Zhang, B. H.; Takeuchi, S. Polym Degrad Stab 2005, 1, 69.
8. Wang, Y. J.; Wang, X. D.; Wei, K.; Zhao, N. R.; Zhang, S. H.; Chen, J. D. Mater Lett 2007, 4–5, 1071.
9. Wang, Y. J.; Huang, W.; Ren, L.; Chen, X. F.; Ke, Y. Chinese Sci Bull 2009, 17, 2940.
10. Ma, Y. J.; Yao, X. F.; Zheng, Q. S.; Yin, Y. J.; Jiang, D. J.; Xu, G. H.; Wei, F.; Zhang, Q. Appl Phys Lett 2010, 97, 061909.
11. Iijima, S. Condens Matter Phys 2002, 323, 1.
12. Coleman, J. N.; Cadek, M.; Ryan, K. P.; Fonseca, A.; Nagy, J. B.; Blau, W. J.; Ferreira, M. S. Polymer 2006, 47, 8556.
13. Smith, C. J.; Shaw, B. J.; Handy, R. D. Aquat Toxicol 2007, 82, 94.
14. Krul, L. P.; Volozhyn, A. L.; Belov, D. A.; Poloiko, N. A.; Artushkevich, A. S.; Zhdanok, S. A.; Solntsev, A. P.; Krauklis, A. V.; Zhukova, I. A. Biomol Eng 2007, 24, 93.
15. Sandler, J.; Shaffer, M.; Prasse, T.; Bauhofer, W.; Schulte, K.; Windle, A. Polymer 1999, 40, 5967.
16. Zhou, Y. X.; Pervin, F.; Lance, L.; Shaik, J. Mater Sci Eng A 2007, 15, 657.
17. Li, S. N.; Li, Z. M.; Yang, M. B.; Hu, Z. Q.; Xu, X. B.; Huang, R. Mater Lett 2004, 30, 3967.
18. Lai, M. F.; Li, J.; Yang, J.; Liu, J. J.; Tong, X.; Cheng, H. M. Polym Int 2004, 53, 1479.
19. Sanchez-Garcia, M. D.; Lagaron, J. M.; Hoa, S. V. Comp Sci Tech 2010, 70, 1095.
20. Chan, K. H. K; Wong, S. Y.; Tiju, W. C.; Li, X.; Kotaki, M.; He, C. B. J Appl Polym Sci 2010, 116, 1030.
21. Davis, V. A.; Parra-Vasquez, A. N. G.; Green, M. J.; Rai, P. K.; Behabtu, N.; Prieto, V. Nat Nanotechnol 2009, 4, 830.
22. Tong, X.; Zheng, J. J.; Lu, Y. C.; Zhang, Z. F.; Cheng, H. M. Mater Lett 2007, 61, 1704.
23. Song, W. H.; Kinloch, I.; Windle, A. Science 2003, 302, 1363.
24. Wei, G. Y.; Zheng, Y. D.; Lv, H. X.; Xi, T. F. J Mater Sci Eng (Chinese) 2009, 27, 355.
25. Song, W. H.; Windle, A. H. Macromolecules 2005, 38, 6181.
26. Zhang, J.; Zou, H. L.; Qing, Q.; Yang, Y. L.; Li, Q. W.; Liu, Z. F.; Guo, X. Y.; Du, Z. L. J Phys Chem B 2003, 107, 3712.
27. Douglas, B. M.; Naumenko, V.; Kuznetsova, A.; Yates, J. T., Jr.; Liu, J.; Smalley, R. E. J Am Chem Soc 2000, 122, 2383.
28. Li, W.; Bai, Y.; Zhang, Y. K.; Sun, M. L.; Cheng, R. M.; Xu, X. C.; Chen, Y. W.; Mo, Y. J. Synth Metals 2005, 155, 509.
29. Doi, Y.; Steinbuchel, A. Biopolymer (Chinese); Beijing Chemistry Press, Beijing, China, 2005, 190.
30. Galego, N.; Rozsa, C.; Sánchez, R.; Fung, J.; Vázquezd, A.; Tomáse, J. S. Polym Test 2000, 19, 485.
31. Organ, S.; Barham, P. Polymer 1993, 34, 459.
32. Schandler, L. S.; Brinson, L. C.; Sawyer, W. G. JOM 2007, 59, 53.
33. Thomas, B.; Fryman, J.; Liu, K.; Mason, J. J Mech Behav Biomed Mater 2009, 6, 588.
34. Shalel-Levanon, S.; Marmur, A. J Colloid Interf Sci 2003, 262, 489.
35. Ma, Y. X.; Zheng, Y. D.; Wu, J.; Tan J.; Li, W.; Yu, Y. Adv Mater Res 2011, 236–238, 1832.